Elsevier Editorial System(tm) for
Construction & Building Materials
Manuscript Draft

Manuscript Number: CONBUILDMAT-D-18-00341R1

Title: Leaching and Microstructural Properties of Lead Contaminated Kaolin Stabilized by GGBS-MgO in Semi-Dynamic Leaching Tests

Article Type: Research Paper

Keywords: Slag; reactive MgO; leaching test; contaminated soil; solidification/stabilization

Corresponding Author: Professor YanJun Du, PhD

Corresponding Author's Institution: Southeast University

First Author: H.L. Wu

Order of Authors: H.L. Wu; F. Jin; Y.L. Bo; YanJun Du, PhD; J.X. Zheng

Abstract: Ground granulated blast furnace slag (GGBS) is widely used to stabilize soils due to its environmental and economic merits. The strength and durability of reactive MgO activated GGBS (GGBS-MgO) stabilized lead (Pb)-contaminated soils have been explored by previous studies. However, the effects of simulated acid rain (SAR) on the leachability and micro-properties of GGBS-MgO stabilized Pb-contaminated soils are hardly investigated. This research studies the leachability and microstructural properties of GGBS-MgO stabilized Pb-contaminated kaolin clay exposed to SAR with initial pH values of 2.0, 4.0 and 7.0. A series of tests are performed including the semi-dynamic leaching tests using SAR as the extraction liquid, acid neutralization capacity (ANC), mercury intrusion porosimetry (MIP), and X-ray diffraction (XRD) tests. The results demonstrate that as the SAR pH decreases from 7.0 to 4.0, the cumulative fraction leached (CFL) and observed diffusion coefficient (Dobs) of Pb increases significantly. Meanwhile, increasing the GGBS-MgO content from 12% to 18% results in decrease of CFL and Dobs. Further decreasing the SAR pH to 2.0 results in the dissolution-controlled leaching mechanism and more notable increase in CFL regardless of the binder dosage. The differences in the leaching properties under different pH conditions are interpreted based on the cemented soil acid buffering capacity, hydration products and pore size distributions obtained from the ANC, MIP, and XRD tests, respectively.

Research Highlights:

- Leaching is diffusion-controlled at pH 7 and 4 while dissolution-controlled at pH 2
- Observed diffusion coefficient is affected by the SAR pH and binder dosage
- Pb is primarily precipitated as hydrocerussite ($Pb_2(CO_3)_2(OH)_2$) in soil matrix
- ANC and pore structure of the treated soil affect diffusive properties of Pb

Leaching and Microstructural Properties of Lead Contaminated Kaolin Stabilized by GGBS-MgO in Semi-Dynamic Leaching Tests

Hao-Liang Wu, Fei Jin, Yu-Lin Bo, Yan-Jun Du*, Jun-Xing Zheng

Hao-Liang Wu
Ph.D. Student, Jiangsu Key Laboratory of Urban Underground Engineering & Environmental Safety, Institute of Geotechnical Engineering, Southeast University, Nanjing 210096, China. Email: wuhaoliang90@163.com

Fei Jin
Assistant Professor, School of Engineering, University of Glasgow, Glasgow G12 8QQ, UK. Email: leoking1987@gmail.com

Yu-Lin Bo
Previous Master Student, Jiangsu Key Laboratory of Urban Underground Engineering & Environmental Safety, Institute of Geotechnical Engineering, Southeast University, Nanjing 210096, China. Email: boyulin.com@163.com

Yan-Jun Du *
Professor, Jiangsu Key Laboratory of Urban Underground Engineering & Environmental Safety, Institute of Geotechnical Engineering, Southeast University, Nanjing 210096, China. *Corresponding author, Tel.: +862583793729; Fax: +862583795086, Email: duyanjun@seu.edu.cn

Jun-Xing Zheng
Assistant Professor, Department of Civil, Construction and Environmental Engineering, Iowa State University, Ames, IA, 50014, USA. Email: junxing@iastate.edu

Technical Paper Resubmitted to Possible Publication in
Construction and Building Materialsl

Abstract: Ground granulated blast furnace slag (GGBS) is widely used to stabilize soils due to its environmental and economic merits. The strength and durability of reactive MgO activated GGBS (GGBS-MgO) stabilized lead (Pb)-contaminated soils have been explored by previous studies. However, the effects of simulated acid rain (SAR) on the leachability and micro-properties of GGBS-MgO stabilized Pb-contaminated soils are hardly investigated. This research studies the leachability and microstructural properties of GGBS-MgO stabilized Pb-contaminated kaolin clay exposed to SAR with initial pH values of 2.0, 4.0 and 7.0. A series of tests were performed including the semi-dynamic leaching tests using SAR as the extraction liquid, acid neutralization capacity (ANC), mercury intrusion porosimetry (MIP), and X-ray diffraction (XRD) tests. The results demonstrate that as the SAR pH decreases from 7.0 to 4.0, the Pb cumulative fraction leached (*CFL*) and observed diffusion coefficient (D^{obs}) increases significantly whereas the leachate pH decreases. Meanwhile, increasing the GGBS-MgO content from 12% to 18% results in the decrease of *CFL* and D^{obs}. Further decreasing the SAR pH to 2.0 results in the dissolution-controlled leaching mechanism regardless of the binder dosage. The differences in the leaching properties under different pH conditions are interpreted based on the cemented soil acid buffering capacity, hydration products and pore size distributions obtained from the ANC, MIP, and XRD tests, respectively.

Keywords: Slag; reactive MgO; leaching test; contaminated soil; solidification/stabilization

1 Introduction

Numerous abandoned industrial sites worldwide have been found to be contaminated with a wide range of heavy metals [1-7]. These toxic metals such as lead (Pb), zinc (Zn), copper (Cu), and cadmium (Cd), if treated improperly, can pose severe threats to the environment and human health. Considering the fast urbanization and ever-increasing value of the land resources, particularly in the developing countries such as China and India, it is imperative to develop effective and economical technologies to remediate these heavy metal contaminated industrial sites. The ultimate goal is to eliminate their negative environmental impact to the society and improve the mechanical properties of soils to facilitate post-construction. Solidification/Stabilization (S/S) has been widely used to immobilize contaminants and improve the soil properties [2-3, 8]. After S/S, the remediated soils can be reused in-situ as engineering construction materials, which would help on the fast redevelopment of the contaminated site [9-10].

Portland cement (PC) is the most popular binder used in S/S [11]. However, its manufacturing process is associated with high power consumption (5000 MJ/t PC), non-renewable resources usage (1.5 t limestone and clay/t PC) and considerable emissions of carbon dioxide (CO_2), dust, and deleterious gases (SO_2, CO, NO_X) (0.95 t/t PC) [12-13]. Therefore, full or partial replacement of PC by more sustainable industrial by-products (e.g. fly ash and slag) as alternative binders in treating contaminated soil has received ever-increasing popularity. One of the promising alternative binders is alkali-activated slag (AAS) cement using ground granulated

blast furnace slag (GGBS) as the main raw material. However, several drawbacks are associated with the utilization of AAS in S/S including over-rapid setting, difficulty in handing/transporting the caustic alkalis and uneconomical efficiency [12]. To address these issues, reactive magnesia (MgO) has been used as an effective activator for the GGBS [12, 14-16]. Existing studies on the GGBS-MgO binder mainly focus on the strength, durability and microstructural properties of the pastes and stabilized soils [14-16]. The MgO facilities the breakage of Si-O and Al-O bonds in the GGBS to promote the formation of the calcium silicate hydrate (C-S-H) and hydrotalcite ($Mg_6Al_2CO_3(OH)_{16}$)-like phase (Ht) as the main hydration products [17-19] while C-S-H and $Ca(OH)_2$ are the main hydration products in PC stabilized soils [2,21]. The C-S-H and Ht formed would enhance the physical and mechanical properties [14-16, 18] and reduce the leachability of contaminants in heavy metal contaminated soils [16, 20]. Recently, the feasibility of using this binder for stabilizing heavy metal-contaminated soils has been demonstrated both in the laboratory [20] and a field trial [8]. However, to date, no systematic studies exist on the diffusive properties of heavy metals in GGBS-MgO stabilized heavy metal contaminated soils.

Sharma and Reddy [6] indicated that the acid rain may vary from a highly acidic condition (pH = 2.0) to a neutral condition (pH = 7.0). It is reported that the average pH value of the acid rain in Nanjing City, China is about 5.09 with the lowest pH of 2.89 [21-23]. Du et al. [2] and Yun et al. [24] studied the leaching behavior and long-term durability of PC solidified/stabilized heavy metal-contaminated soils under various acid rain conditions. They showed that heavy metals could be released

notably from the stabilized soils with increased acidity. It is expected that due to the different hydration chemistry and reaction products formed in GGBS-MgO and PC binders, the leaching properties of the treated soils exposed to the acid rain would be different. Therefore, it is necessary to comprehensively evaluate the leaching behavior of GGBS-MgO stabilized heavy metal-contaminated soils under different acidic conditions: strongly acidic condition (pH = 2.0), moderate acidic condition (pH = 4.0) and neutral condition (pH = 7.0).

In this study, a series of semi-dynamic leaching tests are performed on lead (Pb)-contaminated kaolin clay using simulated acid rain as the extraction leachant with initial pH values of 2.0, 4.0, and 7.0. The effects of acid rain pH and GGBS-MgO content on the leachability and microstructural properties of the treated soils are studied. The semi-dynamic leaching test results are interpreted by acid neutralization capacity (ANC), mercury intrusion porosimetry (MIP) and X-ray diffraction (XRD). This study provides useful insights for remediating Pb-contaminated kaolin using the GGBS-MgO binder.

2 Materials and Testing Methods

2.1 Materials and sample preparations

Kaolin clay is used as a base soil due to its uniform composition (low organic content, homogeneity and uniform mineralogy) and low cation exchange capacity [1-3, 14]. The basic physiochemical properties of the kaolin clay are summarized in

Table 1. The pH is measured per ASTM D4972 [25] using a pH meter HORIBA D-54. The specific gravity is measured per ASTM D5550 [26]. The Atterberg limits are measured per ASTM D4318 [27]. The kaolin clay is classified as lean clay (CL) based on the Unified Soil Classification System [28]. The moisture content is measured as per ASTM D2216 [29]. The grain size distribution is measured using a laser particle size analyzer Mastersizer 2000.

The physiochemical properties of GGBS and MgO are listed in **Table 2.** The BET specific surface areas of the GGBS and MgO are measured by nitrogen adsorption using Physisorption Analyzer ASAP2020. The chemical compositions of the kaolin clay, GGBS, and MgO are measured using X-ray fluorescence (XRF) as shown in **Table 3**. The reactivity of the MgO is measured as the time duration required for the neutralization of an acidic solution (0.25 M acetic acid in this study) by a certain amount of MgO sample (5.0 g in this study) in which phenolphthalein is adopted as the pH indicator [30]. The mean values of the above tests are presented in **Tables 1** to **3**.

Pb is used in this study because it is a very common toxic heavy metal in contaminated soils [3, 14, 31]. Lead nitrate ($Pb(NO_3)_2$) powder (Chemical Analytical Reagent, Sinopharm Chemical Reagent Co., Ltd.) is dissolved in distilled deionized water (DDW) as stock solutions with predetermined Pb concentrations. The simulated acid rain (SAR), used as the extraction liquid (leachant) in the semi-dynamic leaching test, is prepared by diluting nitric acid (HNO_3) and ammonium sulfate ($(NH_4)_2SO_4$) in the DDW. Prior to adding HNO_3, ammonium sulfate ($(NH_4)_2SO_4$) solution is added to

138 the DDW until the concentration of the sulfate ion (SO_4^{2-}) reaches 0.001 mol/L [2].
139 The stock solutions of SAR are adjusted to three pH value of 2.0, 4.0, and 7.0
140 respectively. SAR with pH of 2.0 represents a strong acid rain in the field [2].

141 Previous studies show that a binder with 9: 1 ratio of GGBS to MgO (dry weight
142 basis) yields relatively higher strength and lower leachability of stabilized
143 contaminated soils [14]. Therefore, the binder consisting of 90% GGBS and 10%
144 MgO (dry weight basis) is prepared. Three binder contents are set as 12%, 15%, and
145 18% (dry weight soil basis) which are typical contents in engineering projects [2]. The
146 water content and the Pb concentration are set as 45% and 2% (i.e., 20000 mg/kg)
147 (dry weight soil basis) to simulate a heavily contaminated site soil [11, 21],
148 respectively. Six mixtures are investigated in total and denoted as GM_iPb_j, where i =
149 content of the GGBS-MgO binder (i.e., 12, 15 or 18), and j = Pb concentration (%, 0
150 or 2).

151 The kaolin clay, GGBS and MgO powders are placed in a plastic bottle and are
152 thoroughly mixed by a bench-top mixer. Then the predetermined volume of $Pb(NO_3)_2$
153 stock solution is added to the plastic bottle and further mixed for 30 minutes by the
154 mixer to sufficiently homogenize the mixture. The mixture is filled into a cylindrical
155 PVC mold (Φ50×H100 mm) in five equal height layers. The mold is vibrated
156 manually after each filling to eliminate air bubbles. After five fillings, the mixture is
157 cured under the standard condition (20±2℃, relative humidity = 95%) for 28 days.
158 In addition, the GGBS-MgO cement paste (GGBS : MgO = 9:1, water : cement = 0.6)
159 is prepared following the same procedure but without adding kaolin clay and

160 $Pb(NO_3)_2$ solution. Totally six identical soil samples are prepared with four samples
161 subjected to the semi-dynamic leaching test, and two samples used for the
162 measurement of specific gravity, water content and density before and after the
163 semi-dynamic leaching test. The crushed and sieved sample was also used for ANC
164 and XRD tests. In addition, one GGBS-MgO paste sample is prepared for XRD test.

165 In the authors' previously studies [2, 14], contaminated soils were prepared by
166 spiking clean soil with heavy metal solution at controlled water content, and cured
167 under controlled condition (20±2℃, relative humidity = 95%) until chemical
168 equilibrium between soil and heavy metal is achieved. The mixture is then thoroughly
169 mixed with binder with designed dosage, compacted under controlled dry density and
170 water content, and cured before subjected to various tests. The soil sample preparation
171 method presented in this study is more time effective but the chemical reaction
172 between Pb and kaolin may not achieve equilibrium, which may influence the
173 leaching characteristic and microstructural properties of the stabilized soils. Further
174 study is warranted to address this aspect.

175

176 **2.2 Testing Methods**

177 The semi-dynamic leaching test is conducted as per ASTM C1308-08 [32]. Four
178 replicate samples are tested with three different extraction leachants with pH = 2.0,
179 4.0, and 7.0, respectively. The ratio of the liquid volume to the solid superficial area is
180 9.5 (mL/cm^2). The leachant is replenished at 2 h, 7 h, 1 d and then daily until 11 d. It
181 is noted that the semi-dynamic leaching test is not conducted for the untreated soil as

a preliminary test shown that the untreated soil specimen disintegrated immediately after soaking in the leachant with pH of 7.0 (i.e., DDW).

The pH value of the leachate before each replenishment is measured using a pH meter HORIBA D-54. An aliquot of the leachate is filtered through a 0.45 μm filter and acidified to pH < 2.0 and the concentration of Pb is measured by inductively coupled plasma optical emission spectrometry (ICP-OES, PerkinElmer Optima 8000). Triplicate measurements of pH and Pb concentration are conducted for each sample and the averaged values are reported. The coefficient of variation (COV) values of the pH and Pb concentration for the triplicate measurements are < 3% indicating the good repeatability of the results. The dry density of each sample is calculated from the measured water content and density of two reduplicate stabilized soils before and after the semi-dynamic leaching test.

The cumulative mass of leached Pb is calculated by the following equation:

$$A_{i,\mathrm{Pb}} = \sum c_i \times V_i \quad (1)$$

where $A_{i,\,Pb}$ = the cumulative mass of leached Pb after i th leaching (mg), c_i = the concentration of Pb after i th leaching (mg/L), and V_i = the volume of the leachate (L), which is 1.66 L in this test. The cumulative fraction of leached mass at time t (CFL) is calculated by:

$$CFL = \frac{A_{i,\mathrm{Pb}}}{m} \quad (2)$$

where m = the total mass of Pb in the specimen (mg). The observed diffusion coefficient (D^{obs}) is calculated using the following equation:

$$D^{obs} = \frac{\pi}{4}\left(\frac{CFL}{\sqrt{t}} \bullet \frac{V}{S}\right)^2 \quad (3)$$

where V = volume of the specimen (cm^3), S = surface area of specimen (cm^2) and t = leaching time (s). Herein, D^{obs} is a retarded observed diffusion coefficient since it represents both diffusive and sportive properties of the soils [3, 33].

ANC test is performed according to the procedures developed by Stegemann and Côte [34]. Approximately 10 g soil is sampled from the hand broken sample cured under the standard condition for 28 days, crushed, sieved (< 100 μm), and mixed with 100 mL distilled water. A series of titration tests are conducted on the soil-distilled water mixture using 0.1 M nitric acid as the extraction liquid. An automatic titrating device (Auto Titrator ZDJ-4A) is used to fill extraction liquid until the leachate pH of mixture achieves the target value. Approximately 10 mL leachate after each titration test is collected and filtered through a 0.45 μm filter, and then the concentration of Pb measured by ICP-OES (PerkinElmer Optima 8000). The COV value of the added acid volume less than 6%. This test is performed in duplicate and the average results are reported.

The slope of the titration curve (i.e., acid added to the soil versus leachate pH is expressed as an index of β by Yong [35]:

$$\beta = -\frac{dC_A}{d\mathrm{pH}} \quad (4)$$

where dC_A (cmol) = the increment of moles of acid added to the soil.

After the semi-dynamic leaching test, one specimen is used for MIP test conducted as per ASTM D4404 [36]. The MIP test is used to determine the pore size

distribution of the soil-binder mixture. Approximate 1 cm^3 soil sample is collected from the specimen's surface to the same depth by carefully cutting with a stainless steel knife. Then the collected samples are frozen by the liquid nitrogen (boiling point is -195℃). The frozen samples are dried in a vacuum chamber under -80℃. The MIP tests are performed on dried samples using an Auto Proe IV 9510 mercury intrusion porosimeter. The pore diameter is calculated using the following capillary pressure equation according to ASTM D4404 [36]:

$$d = -\frac{4\tau \cos \alpha}{p} \quad (5)$$

where d (μm) = pore diameter; τ (N/m) = the surface tension; α (°) = contact angles of mercury with the solid; and p (N/m^2) = applied pressure of mercury intrusion. In this study, the contact angle is set as 139° and surface tension value is set as 4.84×10^{-4} N/mm.

The XRD tests are performed on samples of GGBS-MgO paste and 18% GGBS-MgO stabilized kaolin spiked with 2% Pb that are cured under the standard condition for 28 days. Prior to the XRD analysis, 10 g sample is collected, air dried, ground, and sieved (< 0.075 mm), and frozen using liquid nitrogen (-195℃) to be dried by sublimation of the frozen water at -80℃. The XRD test is conducted on gold-coated samples on RigakuD/Max-2500 using a Cu-Kα source with a wavelength of 1.5405 Å. The instrument is operated at 40 kV and 20 mA. A step size of $2\theta = 0.02^{\circ}$ and a scanning speed of 5 s/step are used in the step scan mode. Samples are analyzed over a range of 2θ from 10° to 50°. The binder content, curing time, Pb concentration and number of replicate samples for the various tests are summarized in **Table 4**.

3 Results and Analyses

3.1 Dry Density

Table 5 shows the properties of the Pb-contaminated kaolin clay treated by different contents of GGBS-MgO before the semi-dynamic leaching test. The water content and porosity slightly decrease with increasing content of GGBS-MgO, whereas dry density values are practically the same regardless of GGBS-MgO content. **Tables 6** and **7** present the dry density and normalized dry density after leaching under different SAR pH conditions. It is shown that the change of both dry density and normalized dry density are insignificantly with GGBS-MgO content or SAR pH.

3.2 Cumulative Fraction Leached and Leachate pH

Fig. 1 shows the evolution of the cumulative Pb fraction (*CFL*) and leachate pH with time for samples with different GGBS-MgO contents under SAR pH = 2.0, 4.0, and 7.0 . It can be seen that the *CFL* gradually increase throughout the entire leaching time. When GGBS-MgO content increases from 12 to 18%, *CFL* decreases regardless of the SAR pH. The binder content only has a marginal influence on the *CFL* when it exceeds 15%. At the same binder content and time, the increments of *CFL* are much more significant when SAR pH decreases from 4.0 to 2.0 than those when SAR pH decreases from 7.0 to 4.0. The observation is consistent with those reported by [2] where PC is used as the binder for stabilizing Pb-contaminated kaolin soil. When the

SAR pH values are 4.0 or 7.0, the leachate pH curves are close to each other and both are approximately 10.5. When the SAR pH decreases from 4.0 to 2.0, a remarkable decrease of the leachate pH to ~2.5 is observed because the amount of the alkaline hydration products formed in the soil matrix is not sufficient to buffer the acid solution.

3.3 Observed diffusion coefficient

The cumulative Pb per cross-section area of the soil is plotted against log (*t*) in **Fig. 2** for different SAR pH values. The slopes of the regression lines are calculated in **Table 8**. According to USEPA (Method 1315), if the slope is close to 1 (slope > 0.65), surface dissolution will be the dominant leaching mechanism. If the slope is close to 0.5 (0.35 < slope $\leqslant$0.65), diffusion is the leaching mechanism. If the slope is lower than 0.35, wash-off occurs (or depletion if it is found in the middle or at the end of the test). This study shows that for SAR pH = 2.0, the leaching mechanism is dissolution while it is diffusion for SAR pH = 4.0 and 7.0. The observed diffusion coefficients (D^{obs}) are in the range of 10^{-18} - 10^{-12} m^2/s, which agree with the results from previous studies [37-41]. The comparisons of D^{obs} for Pb in GGBS-MgO, fly ash, quicklime-sulfate and PC stabilized soils [37-42] are shown in **Fig. 3**. Only a few D^{obs} values exist at leachant pH 2.0 due to the strong dissolution effect. When SAR pH is 4.0 or 7.0, D^{obs} decreases as the GGBS-MgO content increases from 12% to 18%. The main hydration products in the GGBS-MgO binder are calcium silicate hydrate (C-S-H), hydrotalcite-like phases (Ht) and brucite ($Mg(OH)_2$) if there is excess MgO

[20]. The formation of brucite and Ht causes a large solid volume expansion and fill pores in stabilized soils [20], leading to more compacted soil structure [2] and therefore lower D^{obs} with higher binder dosages. When the SAR pH decreases from 7.0 to 4.0, the more aggressive SAR attack on the hydration products leads to their gradual dissolution and consequently higher porosity (see "MIP test" section), resulting in slightly higher D^{obs}.

3.4 Acid neutralization capacity

Fig. 4(a) illustrates the titration curves for Pb-contaminated kaolin clay treated by GGBS-MgO. Before adding the acid, the soil with 12% GGBS-MgO binder displays a slightly lower leachate pH than that of the soil with 18% GGBS-MgO binder (i.e., soil pH = 9.9 versus 10.3). Higher GGBS-MgO binder content increases the initial soil pH and thereby could increase the resistance against acid attack. **Fig. 4(b)** shows the values of β computed by **Eq. (4**). Values of β gradually decrease with leachate pH dropping from 10.0 to 5.0. The leachates with pH lower than 5.0 are not appropriate for evaluating the buffering capacity of the contaminated kaolin in this study since a certain amount of soil minerals might have dissolved in the ANC test [35]. Du et al. [14] stabilized Zn and Pb contaminated soils with a phosphate-based binder and observed the turning point of β occurs at the leachate pH of 5.0. In **Fig. 4(b)** the turning point of β is around 7.0 which is slightly higher than Du et al. [14] because the kaolin clay used in this study has less organic component and therefore less acid buffer capacity than natural clay used by Du et al. [14]. **Fig. 4(c)** shows the variation

311 of the leached Pb concentration (μg/kg dry soil) with leachate pH obtained from the
312 ANC test. When the leachate pH is in the range of 2.0 to 4.0, leached Pb
313 concentration decreases noticeably with the increasing GGBS-MgO content or pH. In
314 contrast, leached Pb concentration is lower than 0.015 μg/kg and the values are
315 practically the same when the leachate pH ranges from 5.0 to 10.0 regardless of the
316 GGBS-MgO content or leachate pH.

317

318 **3.5 Pore size distribution**

319 **Fig. 5** presents the cumulative pore volumes for the Pb-contaminated kaolin clay
320 treated by 12% and 18% GGBS-MgO under different pH conditions. Under the same
321 SAR pH condition, the specimens stabilized with 12% GGBS-MgO have notably
322 larger cumulative pore volume than the specimens stabilized with 18% GGBS-MgO.
323 At the same GGBS-MgO content, the cumulative pore volume decreases as the SAR
324 pH increases, which is more noticeable when SAR pH decreases from 4.0 to 2.0.

325 **Fig. 6** shows the pore volumes for pore diameters in different ranges: < 0.01 μm
326 (intra-aggregate), 0.01 to 10 μm (inter-aggregate) and > 10 μm (air pores) respectively.
327 This classification of pore sizes is suggested by Horpibulsuk et al. [43] for the cement
328 and fly ash-stabilized silty clay. The volume percentages of above classified pores are
329 shown in **Table 9**. Regardless of the GGBS-MgO content, the proportions of air pores
330 and intra-aggregate pores increase (more noticeable for air pores), whereas those of
331 inter-aggregate pores decrease when the SAR pH decreases from 7.0 to 2.0.
332 Increasing GGBS-MgO content is found to decrease the proportions of air pores while

increase those of inter- and intra-aggregate pores.

3.6 X-ray diffraction analysis

XRD tests are conducted on the GGBS-MgO paste and 18% GGBS-MgO stabilized kaolin spiked with 2% Pb to investigate the emerging reaction products in the GGBS-MgO paste and stabilized Pb-contaminated kaolin. The results are presented in **Fig 7**. For GGBS-MgO paste samples, the characteristic peaks of Ht at $2\theta \approx 11.5^{\circ}$ and 22.9° agree well with the findings of other researchers [20, 44]. In addition, C-S-H has been detected at $2\theta \approx 29.8^{\circ}$, 31.6°, 38.0° and 48.7°. The C-S-H has lower ratio of calcium and silicon, and therefore its peak is close to the calcite ($CaCO_3$) ($2\theta = 29.8^{\circ}$) as reported by previous studies [20, 44]. MgO is identified suggesting that it has not been fully consumed after 28 days of curing. For Pb-contaminated kaolin treated with 18% GGBS-MgO, the 2θ values of the C-S-H and Ht are found at ~31.7° and 11.3° respectively. The characteristic peak of quartz (SiO_2) has been detected at $2\theta \approx 33.6^{\circ}$. The 2θ of the kaolinite is detected at $2\theta \approx 12.6^{\circ}$, 19.8° and 34.8°. Additionally, a trace peak of lead carbonated hydroxide hydrate (hydrocerussite, $Pb_2(CO_3)_2(OH)_2$) has been detected at $2\theta = 34.2^{\circ}$, which agrees well with Jin and Al-Tabbaa (2014a) [20] that the main immobilization mechanism for Pb by GGBS-MgO binder is the formation of hydrocerussite.

4 Discussion

This study demonstrates that the SAR pH and GGBS-MgO content affect

considerably the leachability and D^{obs} of Pb and microstructural properties of the GGBS-MgO stabilized Pb-contaminated kaolin clay. The mechanisms controlling the variation of these features are summarized as follows:

(1) As the SAR pH decreases from 7.0 to 2.0, the hydration products (C-S-H and Ht) and kaolin might have been gradually dissolved although it is not explored in this study. The treated Pb-contaminated soils subjected to the acidic conditions (pH 4.0 to 2.0), therefore, possess looser structures as compared to those subjected to the neutral condition (pH 7.0) (**Fig. 6**). As the GGBS-MgO content increases from 12% to 18%, higher amounts of hydration products have formed in the soil matrix [15] which in turn results in lower leached Pb concentration observed in the ANC test (**Fig. 4(c)**) and reduces the cumulative volume of pores and the proportions of air pores obtained from the MIP analyses (**Fig. 5**). More compact structure leads to lower D^{obs} and *CFL* values of Pb in the stabilized soils [2].

(2) Regarding the relative variations of the pore volumes in different sizes (**Table 9**), it is proposed that: (a) acid attack results in disintegration of the soil-binder aggregates because kaolin particles and hydration products filling the intra-aggregate pores dissolve, and therefore the intra-aggregate pores volume is elevated; (b) the aggregates themselves, which are formed by kaolin-cement clusters, gradually and partially dissolve due to the acid attack, resulting in the transformation of inter-aggregate pores to air pores. Hence, the inter-aggregate pores volume decreases with decreasing SAR pH, whereas the air pores volume increases with decreasing SAR pH.

(3) Different SAR pH conditions and GGBS-MgO contents affect the soil acid buffering capacity (**Fig. 4**). The β values decreases with decreasing pH because the more hydration products are dissolved with more free hydrogen ions (H^+) in the extraction liquid. As the GGBS-MgO content increases from 12% to 18%, a higher concentration of free hydroxyl ions (OH^-) are produced in the soil pores due to cement hydration, resulting in higher β values.

(4) Both soil structure and acid buffering capacity affect *CFL* and D^{obs} of Pb. The above analyses show that soils exhibit loose structures and low β values when SAR pH or GGBS-MgO content reduces, which in turn results in elevated *CFL* values (**Fig. 1**). **Eq. (3)** shows that D^{obs} obtained from the semi-dynamic test has a square relationship with *CFL*. Consequently, D^{obs} values increase with the decreasing SAR pH or GGBS-MgO content (**Table 8**). At a strong acidic condition (pH 2.0), leaching of Pb is controlled by the mineral dissolution process and therefore D^{obs} is not available.

It should be noted that the stabilized soils are cured for 28 d in this study, while it is demonstrated that the mechanical properties/microstructure of GGBS-MgO improve significantly in the long term (> 90 days) [15, 45]. Therefore longer curing time is warranted to fairly evaluate the performance of GGBS-MgO stabilized contaminated soils. Moreover, the tested soil samples are prepared under well-controlled laboratory conditions, so it is suggested that field contaminated soils could be adopted in future studies.

5 Conclusions

This study investigates the effect of acid rain with different pH values on the leaching properties of GGBS-MgO stabilized Pb-contaminated kaolin clay via a series of semi-dynamic leaching tests. The effects of the pH of simulated acid rain (SAR) and GGBS-MgO content on the cumulative fraction leached (CFL), observed diffusion coefficient of Pb and pore size distribution profiles of the soils are investigated. Based on the results obtained from this study, the following conclusions can be drawn:

(1) The changes of dry density and normalized dry density of Pb-contaminated kaolin clay with GGBS-MgO content or acid rain pH are insignificant within the test conditions in this study.

(2) The *CFL* of Pb is notably affected by the simulated acid rain pH and GGBS-MgO content. *CFL* decreases with increasing GGBS-MgO content while increases with decreasing pH, and its increment is more notable at pH 2.0. At pH 2.0, mineral dissolution is found to be the dominant process that controls the leaching of Pb.

(3) The dominant leaching mechanism of Pb is diffusion at pH 4.0 and 7.0. D^{obs} values of Pb decrease with increasing GGBS-MgO content. The results obtained from this study and those reported in the literature demonstrate that D^{obs} values of Pb increases with decreased pH of leachant tested in the leaching tests.

(4) The Pb-contaminated soils with higher GGBS-MgO content display flatter acid neutralization capacity titration curves and higher acid buffer capacity index.

When the leachate pH ranges from 2.0 to 4.0, the leached Pb concentration obtained from the ANC test decreases noticeably with increasing GGBS-MgO content or leachate pH, while it changes insignificantly regardless of GGBS-MgO content or leachate pH when pH is in the range of 5.0 to 10.0.

(5) MIP results show that the cumulative pore volume decreases as the simulated acid rain pH or GGBS-MgO content increases. The volume percentages of air pores and intra-aggregate pores increase while that of inter-aggregate pores decreases with decreased SAR pH. Increasing GGBS-MgO content decreases the volume percentages of air pores while increases those of both inter- and intra-aggregate pores.

(6) Lead is primarily precipitated as hydrocerussite ($Pb_2(CO_3)_2(OH)_2$) in the soil matrix after GGBS-MgO treatment. The acid buffer capacity and pore structure obtained from the ANC test and MIP analyses are essential for interpreting effects of leachant pH and GGBS-MgO content on the leachability and diffusive properties of Pb in the soils tested.

Acknowledgments

Financial support for this research is obtained from the Environmental Protection Scientific Research Project of Jiangsu Province (Grant No. 2016031), National Natural Science Foundation of China (Grant No. 41472258), Natural Science Foundation of Jiangsu Province (Grant No. BK2012022), Key Program of Natural

443 Science Foundation of Jiangsu Province (Grant No.BE2017715), Colleges and
444 Universities in Jiangsu Province Plans to Graduate Research and Innovation
445 (KYLX16_0242), and the Scientific Research Foundation of Graduate School of
446 Southeast University (Grant No. YBJJ1735)..

447

448 **References**

449 [1]. Du, Y.J., Jiang, N.J., Liu, S.Y., Jin, F., Singh, D.N., and Puppala AJ,.2014.
450 Engineering properties and microstructural characteristics of cement-stabilized
451 zinc-contaminated kaolin. Canadian Geotechnical Journal, **51**(3):289–302. doi:
452 10.1139/cgj-2013-0177.

453 [2]. Du, Y.J., Wei, M.L., Reddy, K.R., Liu, Z.P. and Jin, F., 2014. Effect of acid rain
454 pH on leaching behavior of cement stabilized lead-contaminated soil. Journal of
455 Hazardous Materials, **271**, 131-140. doi:10.1016/j.jhazmat.2014.02.002.

456 [3]. Du, Y.J., Wei, M.L., Reddy, K.R., Jin, F., Wu, H.L. and Liu, Z.B., 2014. New
457 phosphate-based binder for stabilization of soils contaminated with heavy metals:
458 Leaching, strength and microstructure characterization. Journal of Environmental
459 Management, **146**, 179-188. doi:10.1016/j.jenvman.2014.07.035.

460 [4]. Yang Y.L., Reddy K.R., Du Y.J., Fan RD 2017. Short-term hydraulic
461 conductivity and consolidation properties of soil-bentonite backfills exposed to
462 CCR-impacted groundwater. ASCE Journal of Geotechnical and
463 Geoenvironmental Engineering. doi: 10.1061/(ASCE)GT.1943-5606.0001877.

464 [5]. Hu, L., Meegoda, J.N., Du, J., Gao, S. and Wu, X., 2011. Centrifugal study of
465 zone of influence during air-sparging. Journal of Environmental Monitoring,
466 **13**(9), 2443-2449. doi: 10.1039/C0EM00594K. 111
467 [6]. Sharma, H.D. and Reddy, K.R., 2004. Geoenvironmental engineering: site
468 remediation, waste containment, and emerging waste management technologies.
469 John Wiley & Sons, Inc.
470 [7]. Yang Y. L., Reddy K.R., Du Y.J., Fan RD., 2017. SHMP amended calcium
471 bentonite for slurry trench cutoff walls: workability and microstructure
472 characteristics. Canadian Geotechnical Journal.doi: 10.1139/cgj-2017-0291.
473 [8]. Jin, F., Wang, F. and Al-Tabbaa, A., 2016. Three-year performance of in-situ
474 solidified/stabilised soil using novel MgO-bearing binders. Chemosphere, **144**,
475 681-688. doi: 10.1016/j.chemosphere.2015.09.046.
476 [9]. Scanferla, P., Ferrari, G., Pellay, R., Ghirardini, A.V., Zanetto, G. and Libralato,
477 G., 2009. An innovative stabilization/solidification treatment for contaminated
478 soil remediation: demonstration project results. Journal of Soils and Sediments,
479 **9**(3), 229-236. doi: 10.1007/s11368-009-0067-z.
480 [10]. Wei, M.L., Du, Y.J., Reddy, K.R. and Wu, H.L., 2015. Effects of freeze-thaw
481 on characteristics of new KMP binder stabilized Zn-and Pb-contaminated soils.
482 Environmental Science and Pollution Research, 22(24), 19473-19484. doi:
483 10.1007/s11356-015-5133-z.
484 [11]. Chen, L., Du, Y.J., Liu, S.Y. and Jin, F., 2010. Evaluation of cement
485 hydration properties of cement-stabilized lead-contaminated soils using electrical

resistivity measurement. Journal of Hazardous, Toxic, and Radioactive Waste, **15**(4), 312-320. doi: 10.1061/(ASCE)HZ.1944-8376.

[12]. Chen, E. Y., and Li, T. Z., 2011. The ecological environmental effect of high quality blast furnace slag power. China Concrete, **5**, 24–28.

[13]. Chen, Q. D., 2001. Use new technology building cement industry of environmental material type. Cement Engineering, **1**, 1–3

[14]. Du, Y.J., Bo, Y.L., Jin, F. and Liu, C.Y., 2016. Durability of reactive magnesia-activated slag-stabilized low plasticity clay subjected to drying–wetting cycle. European Journal of Environmental and Civil Engineering, **20**(2), 215-230. doi:10.1080/19648189.2015.1030088.

[15]. Jin, F., Gu, K. and Al-Tabbaa, A., 2015. Strength and hydration properties of reactive MgO-activated ground granulated blastfurnace slag paste. Cement and Concrete Composites, **57**, 8-16. doi:10.1016/j.cemconcomp.2014.10.007.

[16]. Goodarzi, A.R. and Movahedrad, M., 2017. Stabilization/solidification of zinc-contaminated kaolin clay using ground granulated blast-furnace slag and different types of activators. Applied Geochemistry, **81**, 155-165. doi:10.1016/j.apgeochem.2017.04.014.

[17]. Yi, Y., Liska, M., Al-Tabbaa, A., 2013. Properties of two model soils stabilized with different blends and contents of GGBS, MgO, lime, and PC. Journal of Materials in Civil Engineering, 26, 267-274. doi: 10.1061/(ASCE)MT.1943-5533.0000806.

[18]. Yi, Y., Liska, M., Al-Tabbaa, A., 2014. Properties and microstructure of

GGBS-MgO pastes. Adv. Cem. Res. 26, 114–122. doi: 10.1680/adcr.13.00005.

[19]. Wu, X., Jiang, W., Roy, D. M. 1990. Early activation and properties of slag cement. Cement and Concrete Research, 20(6): 961-974.

[20]. Jin, F. and Al-Tabbaa, A., 2014. Evaluation of novel reactive MgO activated slag binder for the immobilisation of lead and zinc. Chemosphere, **117**, 285-294. doi: 10.1016/j.chemosphere.2014.07.027.

[21]. Du, Y.J., Jiang, N.J., Shen, S.L. and Jin, F., 2012. Experimental investigation of influence of acid rain on leaching and hydraulic characteristics of cement-based solidified/stabilized lead contaminated clay. Journal of Hazardous Materials, **225**, 195-201. doi: 10.1016/j.jhazmat.2012.04.072.

[22]. Liang, J., 2008. A study on effects of acid rain on soil, yield, and quality on farming of crops in Nanjing (Doctoral dissertation, PhD Thesis, Nanjing University of Information Science and Technology).

[23]. Nanjing Environment Protection Administration (Nanjing EPA). 2012. Report on the State of Environment in Nanjing, Nanjing Environment Protection Administration

[24]. Yun, S.W. and Yu, C., 2015. Immobilization of Cd, Zn, and Pb from soil treated by limestone with variation of pH using a column test. Journal of Chemistry, doi: 10.1155/2015/641415

[25]. ASTM. 2001. Standard test method for pH of soils. ASTM standard D4972-01. American Society for Testing and Materials, West Conshohocken, PA.

[26]. ASTM. 2014. Standard test method for specific gravity of soil solids by gas

530 pycnometer. ASTM standard D5550-14. American Society for Testing and
531 Materials, West Conshohocken, PA.
532 [27]. ASTM. 2010. Standard test method for Liquid Limit, Plastic Limit, and
533 Plasticity Index of Soils. ASTM standard D4318-10. American Society for
534 Testing and Materials, West Conshohocken, PA.
535 [28]. ASTM. 2011. Standard Practice for Classification of Soils for Engineering
536 Purposes (Unified Soil Classification System). ASTM standard D2487-11.
537 American Society for Testing and Materials, West Conshohocken, PA.
538 [29]. ASTM. 2010. Standard Test Methods for Laboratory Determination of Water
539 (Moisture) Content of Soil and Rock by Mass. ASTM standard D2216-10.
540 American Society for Testing and Materials, West Conshohocken, PA.
541 [30]. Jin, F. and Al-Tabbaa, A., 2014. Characterisation of different commercial
542 reactive magnesia. Advances in Cement Research, **26**(2), 101-113. doi:
543 10.1680/adcr.13.00004.
544 [31]. Xie, J. and Li, F., 2010. Overview of the current situation on brownfield
545 remediation and redevelopment in China (No. 2933). The World Bank.
546 [32]. ASTM. 2008. Standard Test Method for Accelerated Leach Test for Diffusive
547 Releases from Solidified Waste and a Computer Program to Model Diffusive,
548 Fractional Leaching from Cylindrical Waste Forms. ASTM standard C1308-08.
549 American Society for Testing and Materials, West Conshohocken, PA
550 [33]. Rowe, R.K., Quigley, R.M., Brachman, R.W. and Booker, J.R., 2004. Barrier
551 systems for waste disposal facilities. Spon Press.

552 [34]. Stegemann, J.A. and Cote, P.L., 1991. Investigation of Test Methods for
553 Solidified Waste Evaluation, Appendix B: Test Methods for Solidified Waste
554 Evaluation. Environment Canada Manuscript Series, Document T5-15,
555 Burlington, Ontario, Canada, 49-52.
556 [35]. Yong, R.N., 2000. Geoenvironmental Contaminated Soils, Pollutant Fate,
557 and Mitigation. CRC Press. Taylor & Fracis Group.
558 [36]. ASTM. 2010. Standard test method for determination of pore volume and
559 pore volume distribution of soil and rock by mercury intrusion porosimetry,
560 ASTM Standards D4404-10, 12.01, American Society for Testing and Materials,
561 West Conshohocken, PA.
562 [37]. Liu, Z.P., Du, Y.J., Jiang, N.J., Zhu, J. J., 2013. Leaching properties of
563 cement-solidified lead-contaminated clay via semi-dynamic leaching tests.
564 Chinese Journal of Geotechnical Engineering, **35**(12), 2212-2218.
565 [38]. Moon, D.H. and Dermatas, D., 2006. An evaluation of lead leachability from
566 stabilized/solidified soils under modified semi-dynamic leaching conditions.
567 Engineering Geology, **85**(1), 67-74. doi: 10.1016/j.enggeo.2005.09.028.
568 [39]. Moon, D.H. and Dermatas, D., 2007. Arsenic and lead release from fly ash
569 stabilized/solidified soils under modified semi-dynamic leaching conditions.
570 Journal of Hazardous Materials, **141**(2), 388-394. doi:
571 10.1016/j.jhazmat.2006.05.085.
572 [40]. Moon, D.H., Dermatas, D. and Grubb, D.G., 2010. Release of arsenic (As)
573 and lead (Pb) from quicklime-sulfate stabilized/solidified soils under

574 diffusion-controlled conditions. Environmental Monitoring and Assessment,
575 **169**(1), 259-265. doi: 10.1007/s10661-009-1167-3.
576 [41]. Song, F., Gu, L., Zhu, N. and Yuan, H., 2013. Leaching behavior of heavy
577 metals from sewage sludge solidified by cement-based binders. Chemosphere,
578 **92**(4), 344-350. doi: 10.1016/j.chemosphere.2013.01.022.
579 [42]. Alexander, M., Bertron, A. and De Belie, N., 2013. Performance of
580 cement-based materials in aggressive aqueous environments, RILEM TC
581 211-PAE. Springer, Berlin.
582 [43]. Horpibulsuk, S., Rachan, R., Chinkulkijniwat, A., Raksachon, Y. and
583 Suddeepong, A., 2010. Analysis of strength development in cement-stabilized
584 silty clay from microstructural considerations. Construction and Building
585 Materials, **24**(10), 2011-2021. doi: 10.1016/j.conbuildmat.2010.03.011.
586 [44]. Wang, S.D., and Scrivener, K.L., 1995. Hydration products of alkali
587 activated slag cement. Cement and Concrete Research, **25**(3), 561-571. doi:
588 10.1016/0008-8846(95)00045-E.
589 [45]. Gu, K., Jin, F., Al-Tabbaa, A., Shi, B. and Liu, J., 2014. Mechanical and
590 hydration properties of ground granulated blastfurnace slag pastes activated with
591 MgO–CaO mixtures. Construction and Building Materials, **69**, 101-108. doi:
592 10.1016/j.conbuildmat.2014.07.032.
593

Table Captions

Table 1. Properties of the kaolin soil used in this study

Table 2. Main physico-chemical properties of GGBS and MgO

Table 3. Chemical compositions of the kaolin soil, GGBS and MgO used in this study measure by XRF

Table 4. Binder content, curing time, Pb concentration and number of replicated samples for various tests used in this study

Table 5. Properties of the stabilized soil before the semi-dynamic leaching tests

Table 6. Dry density of samples calculated from the measured density and water content immediately after the semi-dynamic leaching tests

Table 7. Normalized dry density of samples calculated from the measured density and water content immediately after the semi-dynamic leaching tests

Table 8. Calculated D^{obs} values and leaching mechanisms of Pb for the soils tested between 2 h and 11 d

Table 9. Distribution of the pore volume percentage of the Pb contaminated kaolin treated by GGBS-MgO after semi-dynamic tests

611

612 **Table 1. Properties of the kaolin soil used in this study**

Index	Value
pH	8.77
Specific gravity, G_s	2.68
Plastic limit, w_P (%)	14.6
Liquid limit, w_L (%)	29.4
Grain size distribution (%)	
Clay (< 0.002 mm)	21.5
Silt (0.002 to 0.075 mm)	58
Sand (0.075 to 2 mm)	20.5

613

614 **Table 2. Main physico-chemical properties of GGBS and MgO**

Property	Value	
	GGBS	MgO
Alkalinity[a]	1.689	-
Reactivity (s)	-	102
Specific surface area (m^2/g)	0.2932	28.023
pH (liquid to solid ratio = 1:1)	10.96	10.53

615 [a]The alkalinity of the GGBS is defined as the ratio of contents of CaO, MgO, and
616 Al_2O_3 to that of SiO_2
617

618 **Table 3. Chemical compositions of the kaolin soil, GGBS and MgO used in this**

619 **study measure by XRF**

Chemical composition (*wt*%)	Kaolin	GGBS	MgO
CaO	0.36	33.08	0.84
Al_2O_3	39.3	17.9	0.38
MgO	0.06	6.02	96.5
K_2O	0.21	0.64	0.01
SiO_2	52.1	34.3	1.09
Fe_2O_3	3.38	1.02	0.19
SO_3	0.06	1.64	0.26
MnO	0.11	0.28	0.02
TiO_2	1.12	0.92	0.01
Loss on ignition (at 950°C)	3.3	4.2	0.7

620

621 **Table 4. Binder content, curing times, Pb concentration and number of**

622 **replicated samples for various tests used in this study**

Test/ Analysis	Binder content, %	Curing time, days	Pb concentration, %	Number of replicate samples
Dry density	12, 15, 18	28	2	2
Semi-dynamic test	12, 15, 18	28	2	4
ANC [a]	12, 18	28	2	1
MIP [b]	12, 18	28	2	1
XRD [c]	18	28	0, 2	1

623 [a]ANC= Acid neutralization capacity;
624 [b]MIP = Mercury intrusion porosimetry;
625 [c]XRD = X-ray diffraction

626

627 **Table 5. Properties of the stabilized soils before the semi-dynamic leaching tests**

	[a]Specific gravity, G_s	[b]Water content, %	Dry density, ρ_d (g/cm^3)	Porosity, n	Saturation degree, S
GM12Pb2	2.61	41.0	1.26	0.519	0.992
GM15Pb2	2.59	39.7	1.26	0.514	0.973
GM18Pb2	2.55	38.2	1.28	0.498	0.982

628 [a] ASTM D5550(ASTM 2014)
629 [b] ASTM D2216(ASTM 2010)
630

631 **Table 6. Dry density** (g/cm^3) **of samples calculated from the measured density**

632 **and water content immediately after the semi-dynamic leaching tests**

Sample / pH	pH = 2.0	pH = 4.0	pH = 7.0
GM12Pb2	1.20	1.22	1.23
GM15Pb2	1.25	1.25	1.26
GM18Pb2	1.25	1.25	1.26

633
634

635 **Table 7. Normalized dry density (g/cm^3) of samples calculated from the measured**

636 **density and water content immediately after the semi-dynamic leaching tests**

Sample / pH	pH = 2.0	pH = 4.0	pH = 7.0
GM12Pb2	0.96	0.97	0.98
GM15Pb2	0.99	0.99	1.00
GM18Pb2	0.98	0.98	0.99

637

638

639 **Table 8. Calculated D^{obs} values and leaching mechanisms of Pb for the soils tested**
640 **between 2 h and 11 d**

	pH	Slope	R^2	Mechanism	D^{obs} (m^2/s)
GM12Pb2	2.0	0.71	0.992	dissolution	-
	4.0	0.51	0.96	diffusion	1.69×10^{-16}
	7.0	0.44	0.997	diffusion	7.67×10^{-18}
GM15Pb2	2.0	0.8	0.989	dissolution	-
	4.0	0.52	0.972	diffusion	4.90×10^{-17}
	7.0	0.58	0.962	diffusion	5.00×10^{-18}
GM18Pb2	2.0	0.98	0.982	dissolution	-
	4.0	0.6	0.98	diffusion	5.07×10^{-17}
	7.0	0.6	0.948	diffusion	3.77×10^{-18}

641

642

643 **Table 9. Distribution of the pore volume percentage of the Pb contaminated**

644 **kaolin treated by GGBS-MgO after semi-dynamic test**

	GM12Pb2			GM18Pb2		
SAR pH	pH = 2.0	pH = 4.0	pH = 7.0	pH = 2.0	pH = 4.0	pH = 7.0
intra-aggregate pores (%)	1.86	1.80	1.77	2.74	2.00	1.76
inter-aggregate pores (%)	90.76	91.18	91.70	91.00	92.15	93.86
air pores (%)	7.38	7.00	6.53	6.26	5.85	4.38

645

Figure Captions

Figure. 1. *CFL* for Pb and leahate pH for soils with GGBS-MgO contents of (a) 12%; (b) 15%; and (c) 18%

Figure. 2. The plots of cumulative Pb against log (*t*) from the semi-dynamic tests for specimens with GGBS-MgO content of (a) 12%; (b) 15%; and (c) 18%

Figure. 3. Variation of D^{obs} for lead with leachant pH obtained from this study and previously published studies

Figure. 4. (a) Acid titration curves; (b) buffer capacity; and (c) leached Pb concentration of the lead contaminated kaolin clay treated by GGBS-MgO

Figure. 5. Cumulative pore volume of the Pb contaminated kaolin treated by GGBS-MgO after semi-dynamic leaching test

Figure. 6. Pore volume percentage of the Pb contaminated kaolin treated by GGBS-MgO after semi-dynamic test

Figure. 7. X-ray diffractograms of the GGBS-MgO paste and GGBS-MgO treated Pb-contaminated kaolin cured at the normal condition for 28 days

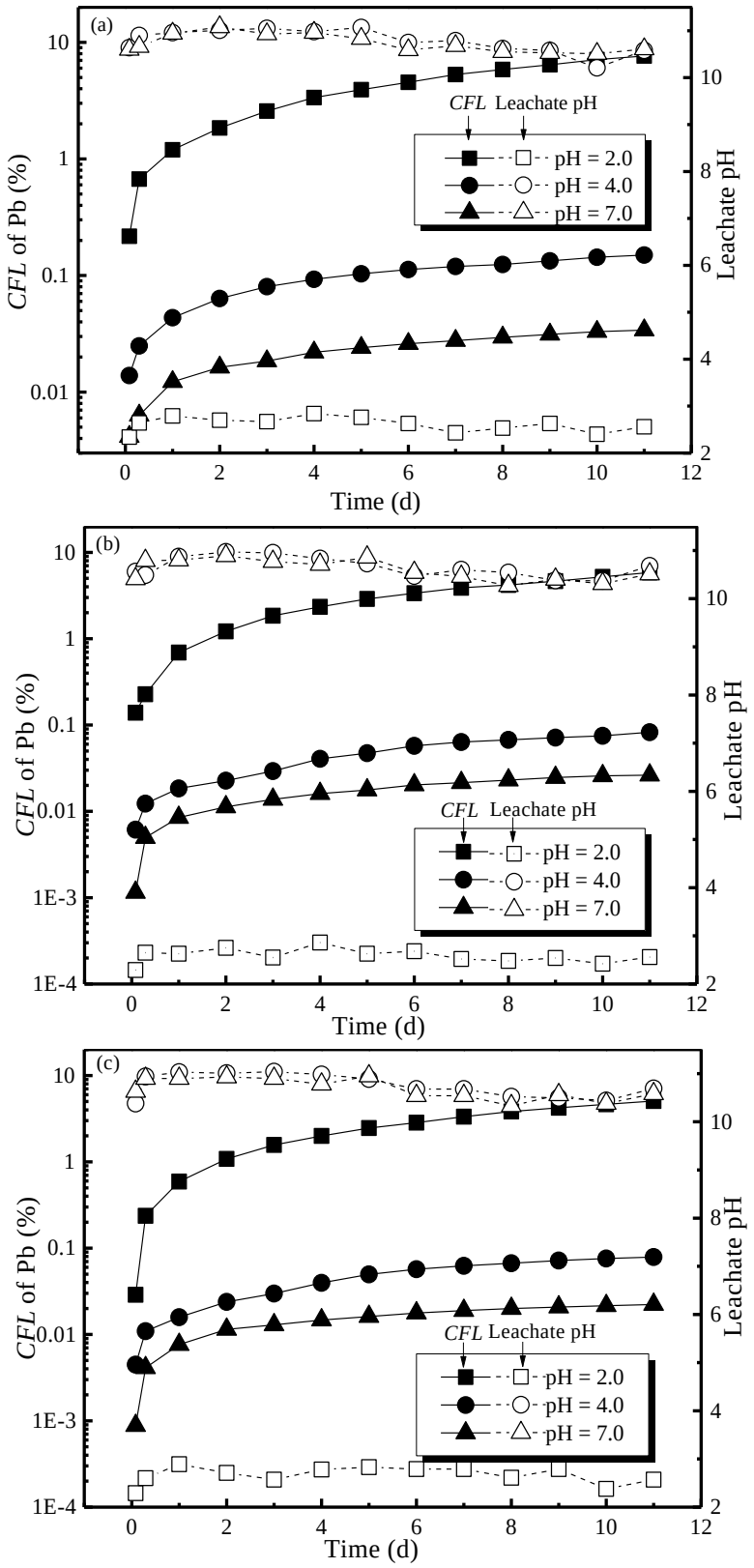

Fig. 1 *CFL* for Pb and leahate pH for soils with GGBS-MgO contents of (a) 12%; (b) 15%; and (c) 18%.

668

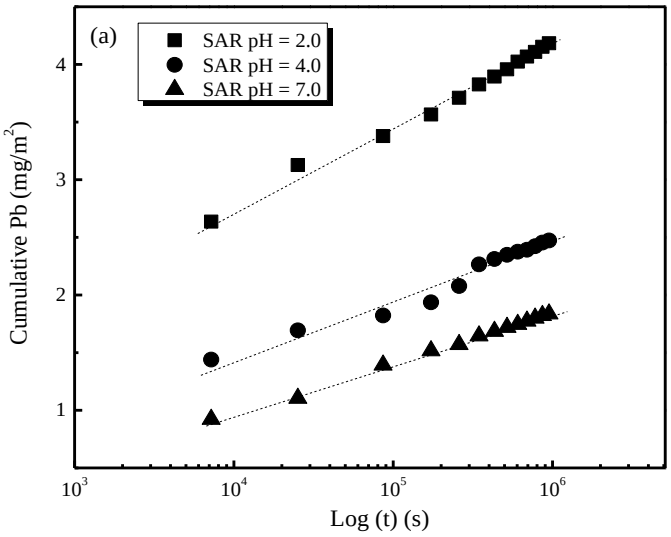

669

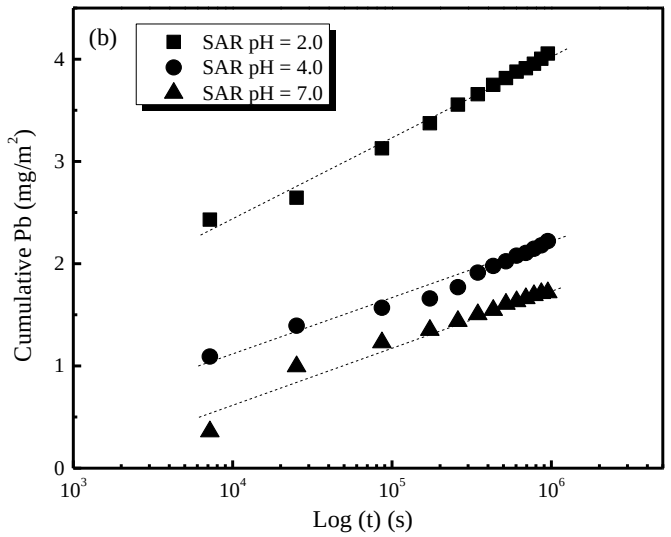

670

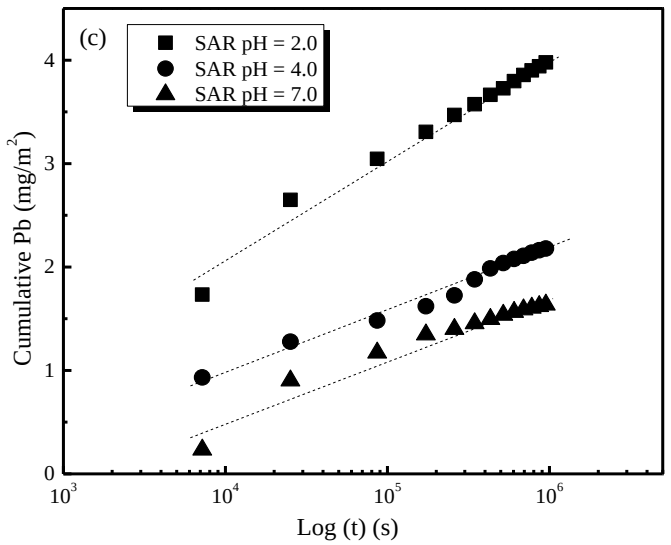

671 **Fig. 2 The plots of cumulative Pb against log (*t*) from the semi-dynamic tests for**

672 **specimens with GGBS-MgO content of (a) 12%; (b) 15%; and (c) 18%.**

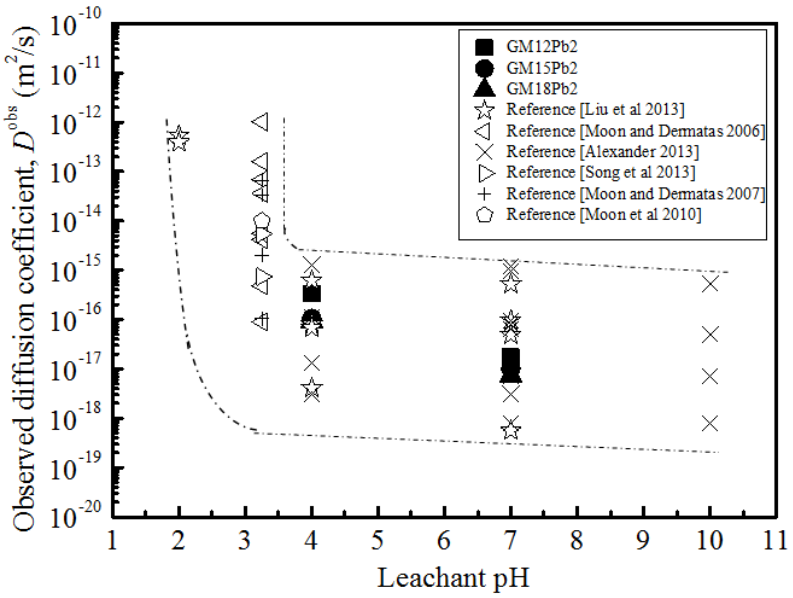

673

674 **Fig. 3 Variation of D^{obs} for lead with leachant pH obtained from this study and**

675 **previously published studies**

676

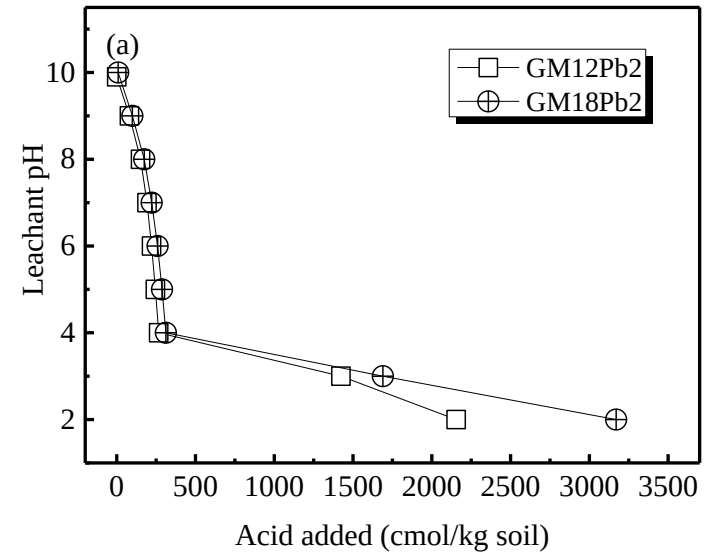

677

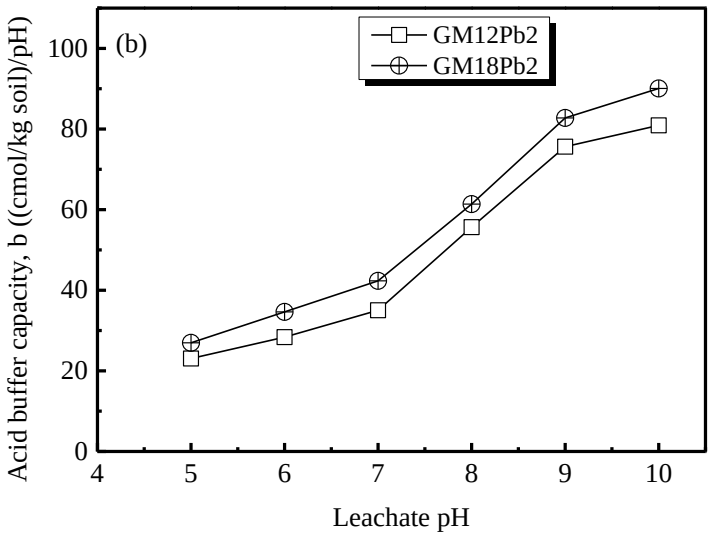

678

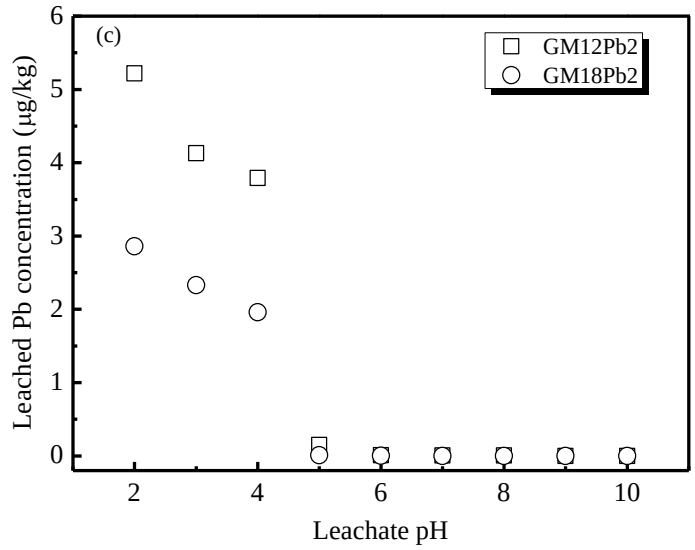

679

680 **Fig. 4 (a) Acid titration curves; (b) buffer capacity; and (c) leached Pb**

681 **concentration of the lead contaminated kaolin clay treated by GGBS-MgO**

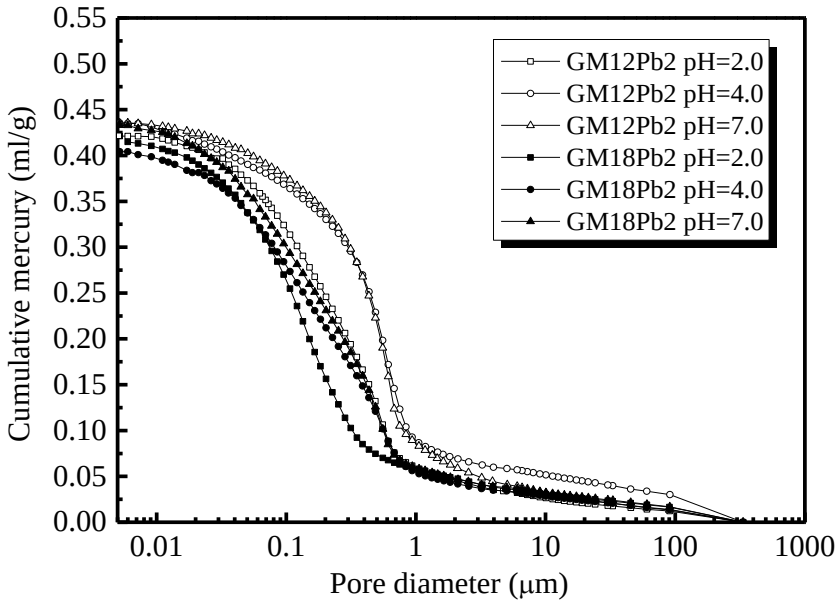

682

683 **Fig. 5 Cumulative pore volume of the Pb contaminated kaolin treated by**

684 **GGBS-MgO after semi-dynamic leaching test**

685

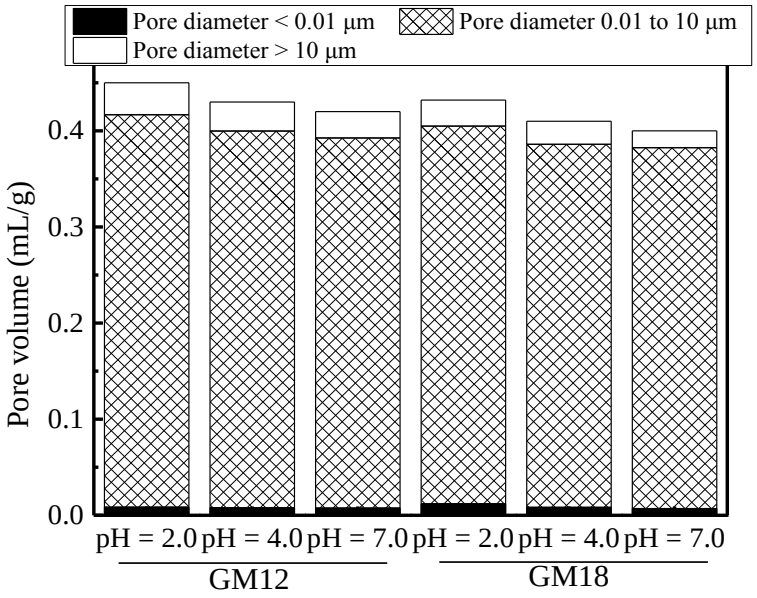

686

687 **Fig. 6 Pore volume percentage of the Pb contaminated kaolin treated by**

688 **GGBS-MgO after semi-dynamic test**

689

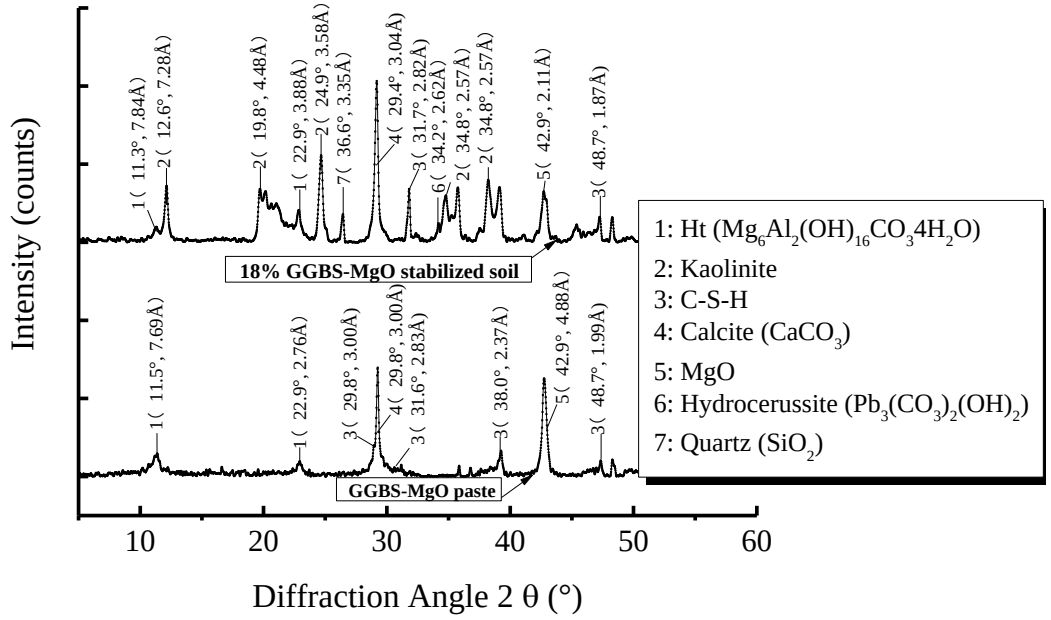

690

691 **Fig. 7 X-ray diffractograms of the GGBS-MgO paste and GGBS-MgO treated**

692 **Pb-contaminated kaolin cured under standard condition for 28 days**

693